

OBSERVED CORE OF A GRADUAL SOLAR ENERGETIC PARTICLE EVENT

L. KOCHAROV¹, M. J. REINER², A. KLASSEN³, B. J. THOMPSON², AND E. VALTONEN¹

¹ Space Research Laboratory, Department of Physics and Astronomy, University of Turku, FI-20014 Turku, Finland

² NASA Goddard Space Flight Center, Greenbelt, MD 20771, USA

³ Institut für Experimentelle und Angewandte Physik, Christian-Albrechts-Universität Kiel, D-24098 Kiel, Germany

Received 2010 July 5; accepted 2010 October 22; published 2010 December 6

ABSTRACT

Using space-borne particle and EUV detection and radio spectrograms from both ground-based and space-borne instruments, we study the first phase of the major solar energetic particle (SEP) event associated with the western solar flare and fast and wide coronal mass ejection (CME) on 2000 April 4. The SEP event being observed at the magnetic connection to the eruption’s center starts with deka-MeV nucl^{-1} helium- and relativistic electron-rich production from coronal sources identified with the electromagnetic diagnostics and the SEP event modeling. The broadband observations and modeling of the initial phase of the “well-connected” major SEP event support the idea that acceleration of SEPs starts in the helium-rich plasma of the eruption’s core in association with coronal shocks and magnetic reconnections caused by the CME liftoff, and that the coronal component dominates during the first hour of the SEP event considered, not yet being shielded by the CME bow shock in the solar wind. The first phase of the SEP event is followed by a second phase of SEP production associated with a decelerating CME-driven shock wave in the solar wind, which accelerates ions from a distinct, helium-poor seed particle population that may originate from the CME interaction with a coronal streamer.

Key words: acceleration of particles – shock waves – Sun: particle emission

1. INTRODUCTION

The abundance of helium in the Sun, solar wind, and energetic particles is critical for many facets of solar physics and being highly variable can contribute to the diagnostics of different solar phenomena (Laming & Feldman 1994; Hansteen et al. 1997; Share & Murphy 1998, and references therein). Using spectroscopic measurements on the *Solar and Heliospheric Observatory* (*SOHO*), the photospheric abundance of helium was determined as $8.5\% \pm 1.3\%$ (Feldman 1998) and the coronal abundance as $5.2\% \pm 0.5\%$ (Laming & Feldman 2001), while the *SOHO*’s coronagraph spectrometer data indicated even lower helium abundance in the coronal streamers, $\text{He}/\text{H} < 4.8\%$ (Raymond et al. 1997).

Solar atmospheric and accelerated helium abundances at the flare site can be determined with γ -ray spectroscopy methods (Kozlovsky & Ramaty 1974; Mandzhavidze et al. 1997, 1999; Share & Murphy 1997, 1998; Murphy et al. 1997). These studies suggest either accelerated ${}^4\text{He}/\text{proton}$ ratios $\gtrsim 50\%$ and/or a higher He/H abundance in the subcoronal regions than in the photosphere. In contrast, long-term measurements of the solar wind typically give smaller He/H ratios. The average ratios in the slow solar wind and in the high-speed streams are 3.5% and 5%, respectively; however, the ratio can be highly variable on short timescales, ranging from 0.1% to over 30% (Neugebauer 1981; Gloeckler and Geiss 1989; Bochsler 1998; Geiss 1998). High helium abundance is observed in the interplanetary space during the passage of the interplanetary counterparts of coronal mass ejections (ICMEs or ejecta) and especially in the ICME’s magnetic clouds, $\text{He}/\text{H} > 8\%$ (e.g., Neugebauer & Golstein 1997; Lynch et al. 2003), which is indicative of the solar environment of the coronal mass ejection (CME) origin. We define an eruption’s core as the helium-rich plasmas of flare site and CME origin.

Early studies of the relative abundance of helium to protons in solar energetic particles (SEPs) were summarized by Van Hollebeke (1975) and Ramaty et al. (1978). In particular it was

found that small events have an abundance of ${}^4\text{He}$ of $\gtrsim 10\%$ relative to protons, whereas in large events the helium-to-proton ratio is typically $\lesssim 1\%$. The difference in the ${}^4\text{He}/p$ abundance observed in SEPs at ~ 10 MeV nucl^{-1} was named among the distinctive properties of the impulsive (small) versus gradual (large) SEP events (e.g., Cliver 1996). The ion acceleration in impulsive events with high He/p has been ascribed to impulsive flares on the Sun, but in gradual events with low He/p to CME shocks in solar wind (Reames 1999).

In this paper, we analyze a large SEP event, where the helium abundance changed from an impulsive-type abundance, $\text{He}/p \gtrsim 10\%$, to a typical value for gradual events, $\text{He}/p \sim 1\%$. We use the helium and proton observations by the Energetic and Relativistic Nuclei and Electron experiment (ERNE) on board *SOHO* (Torsti et al. 1995), the relativistic electron data by *SOHO*/COSTEP/EPHIN (Müller-Mellin et al. 1995), the EUV images by the *SOHO* EUV Imaging Telescope (EIT; Delaboudinière et al. 1995), and dynamic radio spectrograms from the Trestdorf radio spectrometer (Mann et al. 1992) and the WAVES experiment on board *Wind* (Bougeret et al. 1995). A particle transport model will be used to connect these remote and in situ observations.

2. DATA ANALYSIS

We analyze here multiwavelength observations of the first stage of the 2000 April 4–6 event, which is among the major SEP events of solar cycle 23 (Gopalswamy 2003), whereas other stages of that event were described in our previous paper (Kocharov et al. 2009). In that paper, we also reported on the ~ 20 MeV proton angular distributions observed by the high-energy detector (HED) of *SOHO*/ERNE. The observed high, field-aligned anisotropy of the particle flux justifies using a shifted time technique for estimates of SEP spectra and time profiles at the particle source in the rise phase of the event. Figure 1 shows the *SOHO*-observed SEP profiles as functions of the shifted time t_{ES} , where the shifted time or electromagnetic

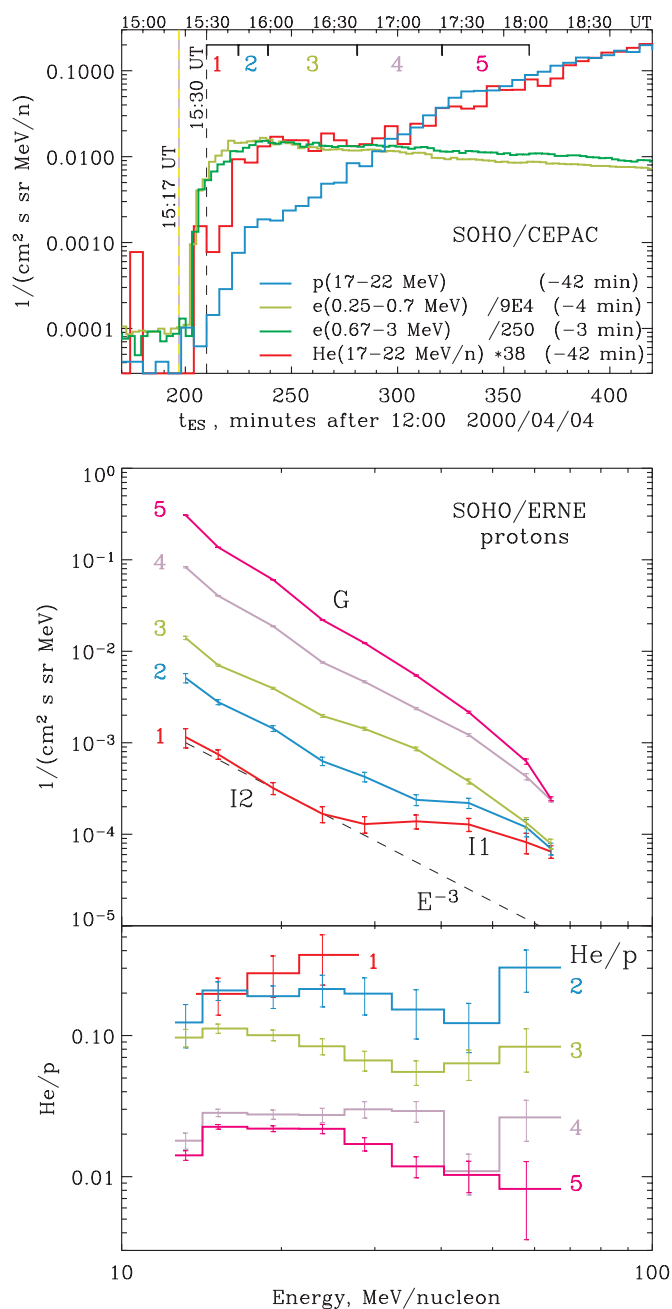


Figure 1. Intensity profiles of deka-MeV $nucl^{-1}$ ions and relativistic electrons during the initial phase of the 2000 April 4 event as a function of the shifted time t_{ES} (uppermost panel); data from COSTEP/EPHIN and ERNE/HED, which are parts of the Costep and Erne Particle Analyser Collaboration (CEPAC). The profiles of protons (blue histogram) and helium (red histogram) were normalized to the same magnitude at the event peak ($t_{ES} = 500-540$ min). Then the two electron profiles (light and dark green curves) were normalized to the helium intensity at around $t_{ES} = 250$ min. The middle panel shows the proton energy spectra for five fixed intervals of the shifted time (intervals 1–5 indicated in the uppermost panel) and the bottom panel shows the corresponding helium-to-proton abundance ratios. It is seen that the SEP production starts with helium- and electron-rich components, $He/p \sim 0.1$, while the second, main stage of production is of a typical gradual composition, $He/p \sim 0.01$.

signature time is the particle observation time at 1 AU minus the time it takes the particle to travel 1.2 AU and plus 8 minutes for a comparison with solar electromagnetic emissions observed from Earth's orbit. The helium intensity–time profile was normalized to the peak intensity of protons. The renormalization method makes it possible to compare rise profiles of different ion species

irrespective of the difference in their pre-event (background) levels. Also shown in Figure 1 are the proton energy spectrum and the He/p abundance ratio for selected periods of the shifted time. Note that after the event's rise phase a shifted intensity profile may deviate sharply from the corresponding solar source profile, so that the time shift may not provide even a rough estimate of the source. The uppermost panel of Figure 1 shows a steep onset of the SEP emission, which first appears above the background level at $t_{ES} = 15:24$ UT (± 2 min) and reveals enhanced abundances of helium and electrons relative to protons lasting for more than an hour (periods 1–3). At the beginning of the event, two distinct spectral components of protons can be seen in the middle panel of Figure 1, components I1 and I2, where “I” stands for impulsive-type composition, $He/p \gtrsim 0.1$ (lower panel). The hardest component, I1, is visible only at very beginning of the event. Later in the event, in periods 4 and 5, the proton energy spectrum evolves to an unbroken, soft spectrum with a typical gradual (G) composition, $He/p \sim 0.01$. Our present research focuses on the SEP event's initial phase from the onset through the end of period 3.

A gradual soft X-ray flare of class C9.7/2F started at 15:12 UT and peaked at 15:41 UT, with $H\alpha$ maximum at 15:33 UT located at N16W66 in NOAA active region 8933. The corresponding halo CME was first observed by the Large Angle and Spectrometric Coronagraph (LASCO) at 16:32 UT. EUV images from *SOHO*/EIT are shown in Figure 2. A difference image in the central panel illustrates the changes associated with onset of the SEP event. A summary sketch is provided in the left panel showing the active region and the CME's footprints—dimming and coronal wave. Coronal dimming in the central panel was imaged right at the peak time of microwave and hard X-ray/ γ -ray bursts, 15:24 UT (flare impulsive phase), close to the time when the first SEPs were released at the root of the Earth-connected interplanetary magnetic line (Figure 1). The coronal dimming and EIT wave extend to south and south-east of the flaring active region, where the interplanetary magnetic connection to Earth is expected, providing prompt access of SEPs to the particle detectors on *SOHO*.

Figure 3 shows a dynamic radio spectrum from the Trens-dorf radio observatory of Astrophysical Institute Potsdam (AIP). The spectrum reveals two episodes of high-frequency (metric) type II emission. The first metric type II burst appears at 15:24–15:27 UT showing the fundamental (40–80 MHz range) and the harmonic (110–160 MHz) lanes. Later, at 15:28–15:32 UT, the presence of strong “herringbone” bursts in the range 40–80 MHz implies a second metric type II burst. “Herringbones” are regarded as signatures of electron beams accelerated at the shock (or another driver) that propagate nearly transverse to the coronal magnetic field (e.g., Mann & Klassen 2005). A full range of radio signatures produced by the acceleration and propagation of low-energy electrons in association with the 2000 April 4 eruption is shown in Figure 4, a composite dynamic radio spectrogram of the ground-based (AIP and Ondrejov) and space-borne (*Wind*/WAVES) observations, comprising data covering the frequency range from 20 kHz to 3 GHz.

The eruption began with a group of strong type III bursts starting at about 15:17 UT at 650 MHz. This onset time is coincident with the start of a microwave event at 3 GHz, which is believed to represent the radio signature of electron acceleration deep in the corona (Bastian et al. 1998). The presence of the metric and kilometric type III bursts indicates that at least some of the low-energy electrons ($\lesssim 10$ keV) were able to escape from

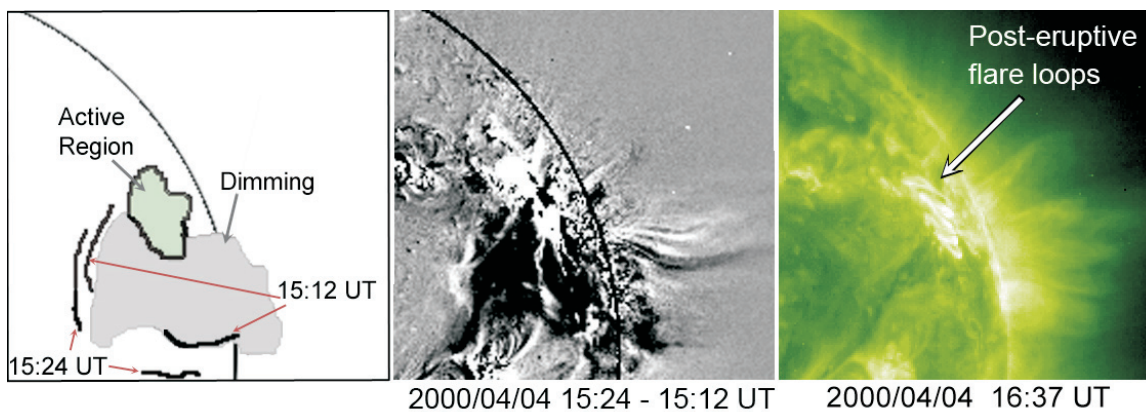


Figure 2. Summary of 195 Å images of the 2000 April 4 flare-CME event provided by *SOHO*/EIT. Right frame is an original image at 16:37 UT illustrating the flare site; shown in the central panel is a difference image between 15:24 UT and 15:12 UT illustrating the CME's footprints; and the sketch in the left panel indicates the flaring active region and summarizes the differences between the images at 15:12 UT and 15:00 UT (coronal wave front at 15:12 UT) and between the images at 15:24 UT and 15:12 UT (coronal wave at 15:24 UT and dimming).

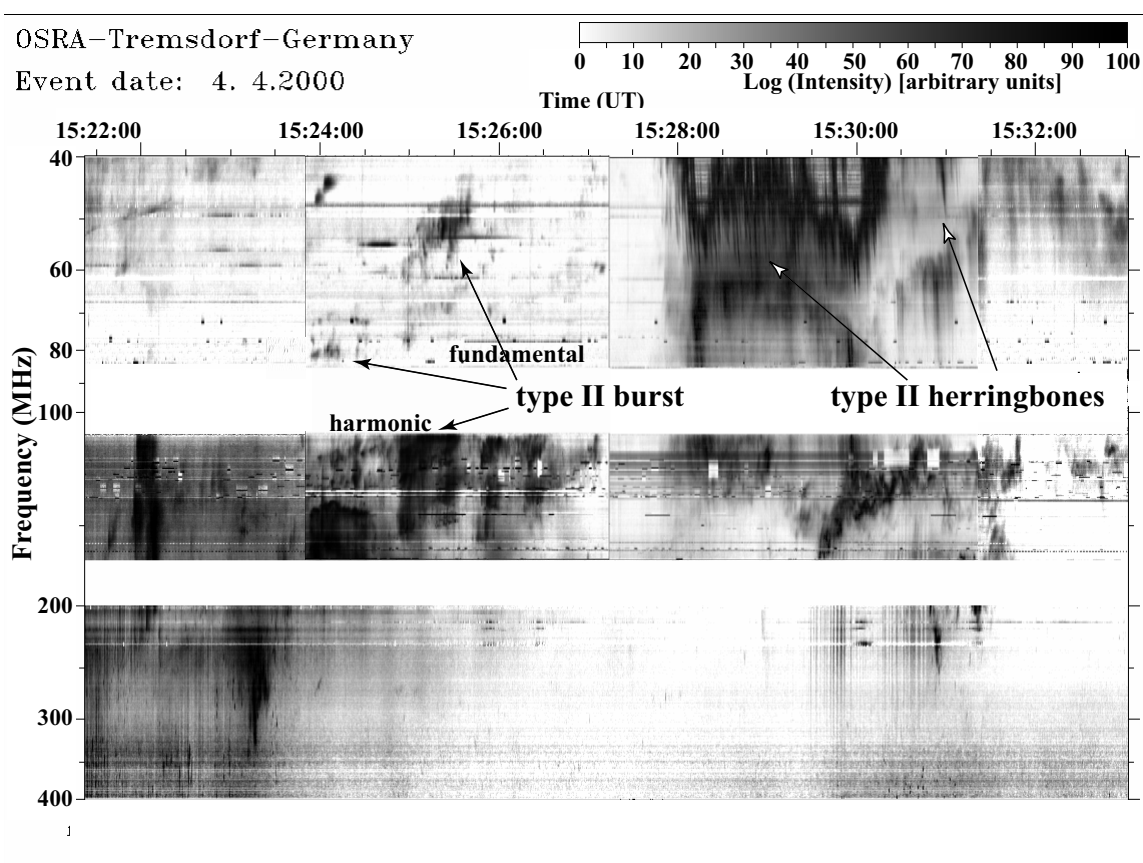


Figure 3. Dynamic radio spectrum of the 2000 April 4 event from the Tremisdorf radio observatory of Astrophysical Institute Potsdam (AIP) revealing two high-frequency type II bursts, one of which possesses a “herringbone” structure. “Herringbone” bursts normally appear as short and fast drifting stripes propagating toward both high and low frequencies. In our case only reverse drifting bursts are seen. The normal drifting bursts should be out of the spectrograph range (<40 MHz). The spectrum close to 40 MHz is partly saturated due to strong radio emission.

the corona and propagate along the magnetic field lines through interplanetary space. This electron injection event lasted for some 30 minutes, with the starting frequency of the individual type III components gradually decreasing with time.

In addition to the complex type III emissions corresponding to the propagation of flare-CME-liftoff associated electron beams through the corona and interplanetary medium, there is also evidence for four type II radio emission events observed during the time interval considered. Two of these type IIs are shown

in Figure 3 (also in the insert to Figure 4). Then, there is a decametric type II at about 15:50 UT at 10 MHz, which is likely the lower frequency continuation of the metric type II. Finally, electrons accelerated by a CME-driven shock propagating through the upper corona and interplanetary medium produced the long-lasting, weak, and diffuse type II radio emissions observed in the decametric and kilometric wavelength band below about 5 MHz. Analysis of this latter type II was previously used by Reiner et al. (2007) to deduce the kinematics of

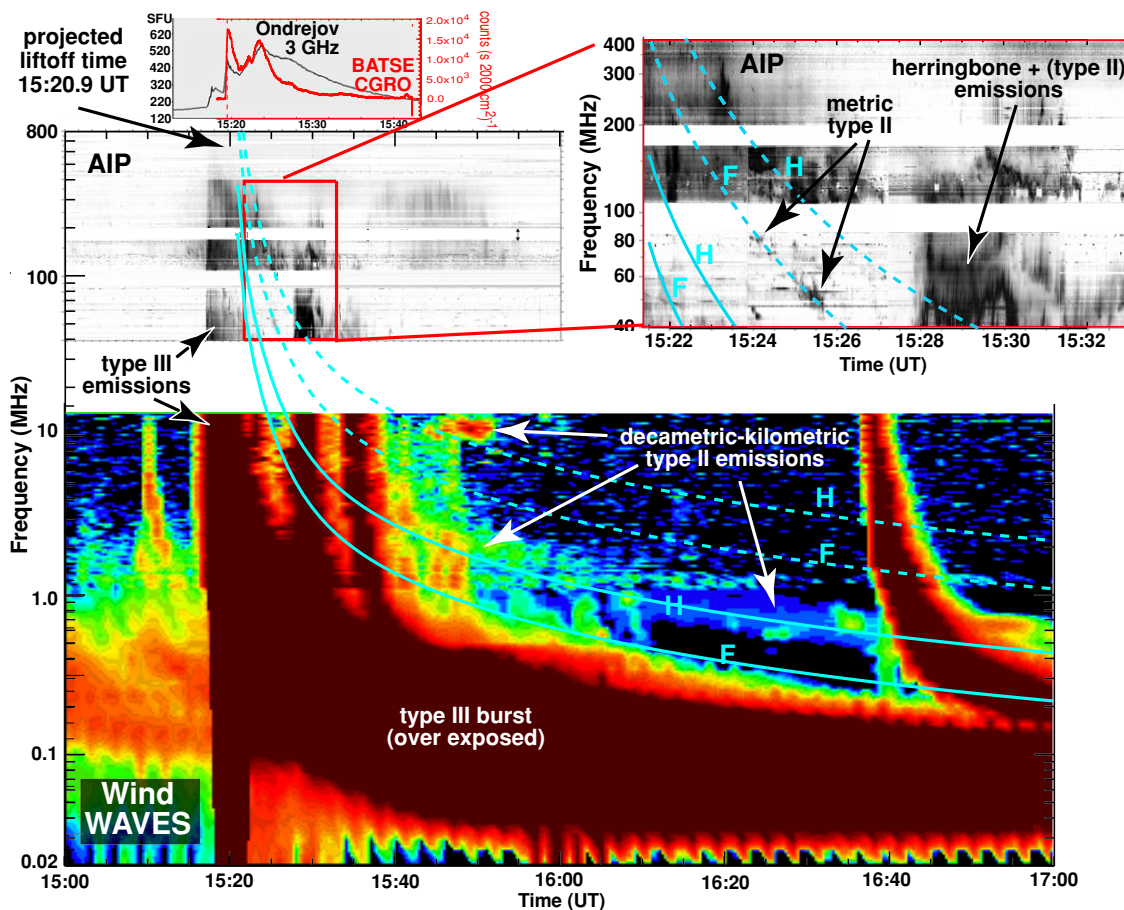


Figure 4. Dynamic radio spectrum of the 2000 April 4 event from the Trensford radio observatory of Astrophysical Institute Potsdam (AIP) and the WAVES experiment on board *Wind*, showing a group of strong type III bursts at 15:17–15:39 UT and a weak group at 15:40–15:50 UT, with starting frequency decreasing with time, and type II radio bursts—metric–decametric (upper, intermittent) and decametric–kilometric (lower, continual). Two lower curves (fundamental, F, and harmonic, H) show a fit to the low-frequency type II with the decelerating shock model of Reiner et al. (2007); initial projected speed is 3400 km s^{-1} and initial deceleration is -99.5 m s^{-2} . The profiles have been extrapolated to the solar corona, using the coronal density model of Saito (1970) renormalized by a factor of 0.9. The two upper curves H and F are for the same shock model but in a dense coronal structure corresponding to the Saito model renormalized by a factor of 24. The insert zooms in on the metric type II and associated herringbone structure. The uppermost panel illustrates the flare impulsive phase with its microwave and hard X-ray (30–58 keV) bursts.

the associated CME, finding an initial projected speed of 3400 km s^{-1} and initial deceleration of -99.5 m s^{-2} . In that work, the high-frequency metric and decimetric radio emissions were not considered.

We do not know whether the metric and decametric–kilometric type II emissions were produced by the same or by different shocks. However, if we make the plausible assumption that both the first metric type II and the kilometric type II emissions were generated by the same CME-driven shock, leaving alternatives for Section 3, then the observed frequency drift of the emissions provides a precise constraint on the projected liftoff time of the corresponding CME. The dashed and solid curves in Figure 4 show the frequency–time profile corresponding to the common shock kinematics assuming the projected liftoff time of 15:20.9 UT. The Saito (1970) coronal density model was used to convert the heliocentric distance to a frequency; the pair curves, labeled F and H, correspond to the radio emissions generated at the fundamental and harmonic of the plasma frequency. In order to simultaneously fit both the metric and kilometric emissions, we had to assume that the common shock propagated through quite different density structures of the corona. We obtained the best fit to the frequency drift of the decametric–kilometric type II emissions for the CME shock

propagating through a region of the corona with density falling off at 0.9 times the Saito model. The best fit to the frequency drift of the first metric type II burst required that the same shock must have propagated through an enhanced density region (such as a coronal streamer) with density falling off at 24 times the Saito model. Type II radio emission generated in enhanced density regions of the corona is suggested by previous work that indicated that such emission may be generated in dense coronal streamers (Reiner et al. 2003, their Figure 5). The fit shown in Figure 4, however, misses the bright drifting emission between 15:29 and 15:31 UT in the 110–160 MHz range, which could indicate another type II (see the insert).

To accurately connect the solar electromagnetic observations to the near-Earth particle fluxes, a more complete SEP transport model than that suggested above for the estimates of Figure 1 is required. A model that accounts for the particle scattering at MHD turbulence in the solar wind flow and focuses on a realistic magnetic environment for the 2000 April 4 event was formulated by Kocharov et al. (2009), based on a general model by Kocharov et al. (2005) and on the peculiarities of the $\sim 20 \text{ MeV}$ proton pitch-angle distribution observed by the particle telescope ERNE/HED on *SOHO* during the first six hours of this SEP event. The interplanetary magnetic field model

comprises a piece of Archimedean spiral between the Sun and the Earth, a magnetic mirror (“bottle neck”) behind the Earth, and a round arch of angular span Φ behind the mirror. The behind-Earth magnetic mirror showed up in the bounced particle flux observed in this SEP event (Figure 1(e) of Kocharov et al. 2009). The model simplifies a magnetic field line draping around the western flank of the interplanetary extension of a previous “old” CME (Figure 3 of Kocharov et al. 2009).

Based on the observed steepness of the pitch-angle distribution of outward streaming protons, we estimate the mean free path value to be 2.5 AU for a 10 MeV proton near Earth’s orbit. Then we adopt the mean free path value of 3.15 AU for a 10 MeV nucl^{-1} alpha particle, based on the quasilinear theory scaling for the Kolmogorov turbulence spectrum. Unfortunately, flux anisotropy data for relativistic electrons are missing. However, there is a theoretical estimate that the mean free path of MeV electrons should be slightly lower than that of 10 MeV protons (Bieber et al. 1994, Figure 10). For simulations of the electron transport, we take the 1 MeV electron mean free path to be 1.5 AU and assume that in the energy range 0.25–3 MeV it varies as the reciprocal of the electron’s speed. The round arch angular span $\Phi = 60^\circ$ is adopted. We add an extra degree of freedom to the model by allowing the particle mean free path in the round arch to be either the same value as in the Archimedean spiral (Model 2) or reduced by a factor of 10 (Model 1), both still consistent with proton pitch-angle distributions observed during the first six hours of the event. The additional degree of freedom affects mainly the high-speed electrons and will serve to illustrate the uncertainties in the electron data fitting.

A rapid change in the observed ratio between the two energy channels of relativistic electrons at the time indicated by the vertical yellow line in the lowermost panel of Figure 5 suggests a corresponding change in the electron energy spectrum, which implies that at least two electron injection sources exist at the Sun. Being not associated with any prominent local changes in the solar wind, the electron spectrum change is attributed to a temporal change in the electron source at the Sun. The two upper panels of Figure 5 show the results of the SEP transport simulations for the 0.25–0.7 MeV and 0.67–3 MeV electron intensity–time profiles with a double source model: the first source with energy spectrum $E^{-5.7}$ (red curve) and the second source with spectrum $E^{-5.3}$ (blue curve). The time profiles and spectra of the sources have been adjusted so that the results of the SEP transport simulations accurately reproduce the rise phase of the observed intensity profile at $t_{\text{ES}} = 200$ –220 min (green curves in the upper panels of Figure 5) and the channel ratio change at $t_{\text{ES}} = 220$ –240 min (lowermost panel). However, fitting the event’s decay phase is ambiguous because of the lack of electron anisotropy data. Interplanetary transport Model 1 (upper panel) results in the solar relativistic electron production proceeding only during the first 35 minutes, whereas in Model 2 (middle panel) the larger mean free path value assumed in the round arch leads to a tail in the electron production profile after the first 40 minutes. Irrespective of details of the interplanetary transport model, note a remarkable agreement between the first production period of relativistic electrons, 15:17–15:39 UT (red source), and the strong type III bursts of Figure 4, with possible ≈ 3 min inaccuracy in the electron data fitting.

Modeling results for the 17–22 MeV nucl^{-1} helium are shown in Figure 6, where we have fitted with Model 1 only the initial part of the SEP event. In contrast to electrons, a tail in the helium-rich component is obscured by the new intensity rise and could not be investigated.

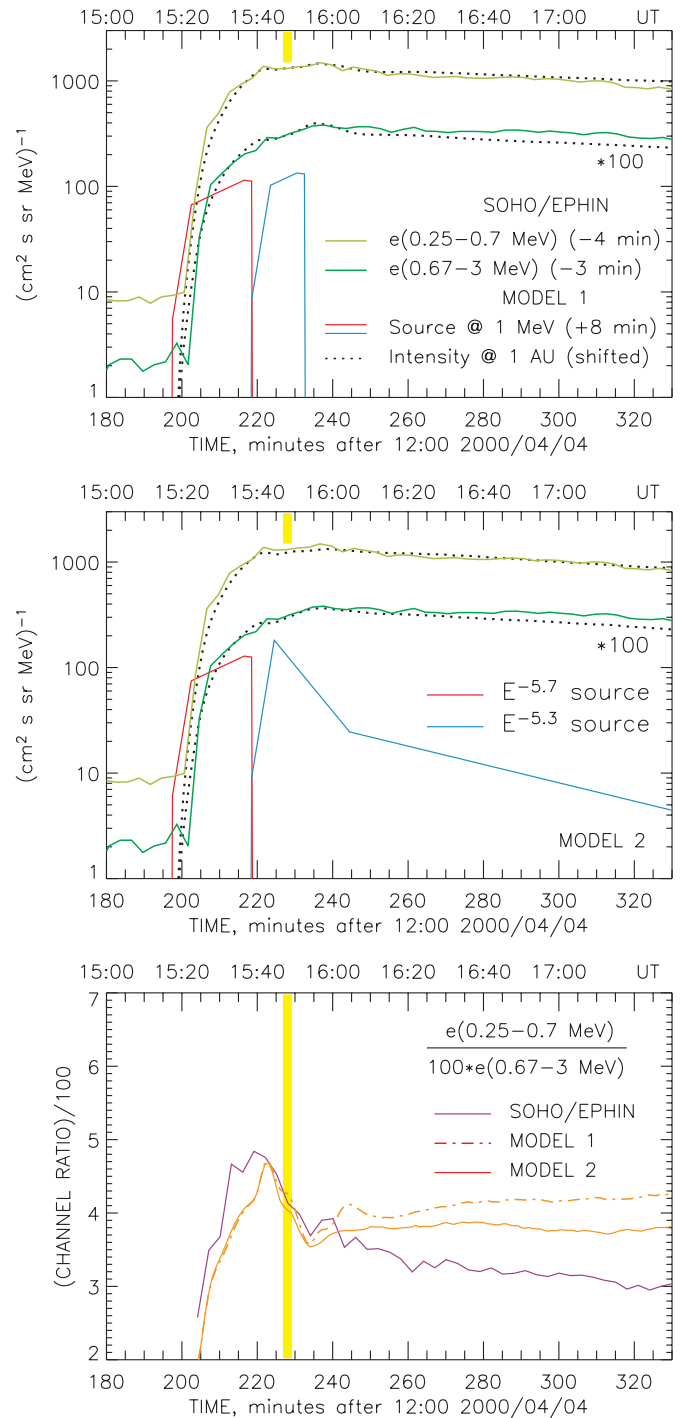


Figure 5. SEP modeling results for two models of the 2000 April 4 electron event, Model 1 and Model 2 (two upper panels): the model source functions of relativistic electrons at the Sun (red and blue curves; shifted by +8 min) and the simulated intensity–time profiles at 1 AU (dotted black curves) superposed on the 3 min average intensity profiles observed on *SOHO* (dark and light green curves); all are plotted as functions of the shifted time t_{ES} . The lowermost panel shows the corresponding profiles of the electron intensity ratio between the two energy channels of *SOHO*/EPHIN. The two upper panels additionally illustrate that a simple time shift of the near-Earth-observed SEP intensity–time profile could be used for rough estimates of only a rise phase of the SEP source.

3. DISCUSSION

Our data for the western event of 2000 April 4 reveal a helium-rich beginning with falling He/ p ratio after the first hour of the event (Figure 1). Reames et al. (2000) reported that there have

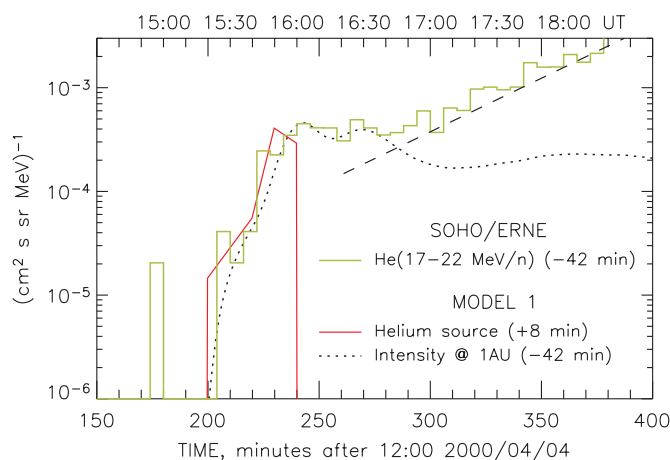


Figure 6. Modeling of the first stage of the 2000 April 4 energetic helium event: model source function of deka-MeV nucl^{-1} helium (red curve; shifted by +8 min); the simulated intensity profile at 1 AU as a function of the shifted time t_{ES} (dotted black curve); and the intensity–time profile observed on *SOHO*, also shifted in time (green histogram). The dashed line indicates a rise of the second stage of production (not modeled).

been observations of both falling and rising He/p time profiles at the beginning of SEP events (also Cohen et al. 2005; Mason et al. 2006). The rising He/p profiles were explained by the ion propagation through the proton-amplified waves expected in the strongest events (Ng et al. 1999), a pattern not observed in the 2000 April 4 event. Large SEP events produced on the Sun’s western hemisphere typically have enhanced event-averaged abundances of heavy ions in the deka-MeV nucl^{-1} energy range (Cane et al. 2003, 2006), while intensity profiles and elemental abundances show a complex variation with time (Klecker et al. 2006). Our high-resolution observations of the 2000 April 4 event have revealed three components of SEPs, two of which were produced in the beginning of the event—the helium-rich components I1 and I2 of Figure 1. They could be attributed to an acceleration in the complicated magnetic environment of the solar corona.

In a correlative study between >20 MeV solar proton events, CMEs, flares, and radio bursts, Cane et al. (2002) found that essentially all of the proton events are preceded by groups of type III bursts, with the type III’s starting frequencies decreasing as a function of time. Recently, unrelated to SEPs, Cohen et al. (2009) have analyzed a coronal (EIT) wave–CME-dimming event using a three-dimensional, global magnetohydrodynamic model for the solar corona and found evidence that CME expansion is facilitated by magnetic reconnection between the expanding CME core and the surrounding magnetic environment, which leads to the “opening” of coronal field lines on a global scale.

The 2000 April 4 SEP event started on the Sun simultaneously with the appearance of the CME footprints—coronal wave and dimming observed by *SOHO*/EIT (Figure 2). Magnetic field line “opening” associated with the CME core rise could provide a way out for the high-energy particles accelerated near the CME origin. An initial period of the SEP emission is associated with intense type IIIs with starting frequencies that decrease as a function of time in concert with a frequency-drifting metric–decametric type II burst (Figure 4). Another, low-frequency type II observed by *Wind*/WAVES was produced by the CME bow shock in less dense coronal regions. Those electromagnetic signatures are consistent with the paradigm of the CME core expansion and concurrent coronal field line

opening, when the type III electrons are emitted in the vicinity of the CME core behind its bow shock, overtake the shock and escape into the interplanetary space.

As pointed out above in Section 1, a helium-rich material for the SEP acceleration exists at the CME origin at the Sun, which could be named the CME’s helium-rich core. The inferred source profile of energetic helium and the relativistic electron source are similar to each other, and even two sub-sources of relativistic electrons find their counterparts in the structure of the helium source (Figure 5 versus Figure 6). On the other hand, the timing of the relativistic electron source fits well with the type III radio bursts shown in Figure 4. Type III electron beams start in the vicinity of the high-frequency type II structure, then overtake the low-frequency type II shock and propagate further to the interplanetary space. A straightforward interpretation of these remarkable correspondences could be a simultaneous release of both low-energy and relativistic electrons and helium-rich SEPs at magnetic reconnections in the course of the upward motion and expansion of the CME’s helium-rich core, progenitor of the helium-rich ejecta in space. During the first ≈ 40 min of the SEP event at the Sun, until $t_{\text{ES}} \approx 16:00$ UT, the accelerated particles from the helium-rich core were not shielded by the interplanetary CME-driven shock and had access to the solar wind upstream of the shock. Those particles dominated at 1 AU during the first ≈ 1.5 hr of the event.

The bow shock of the 2000 April 4 CME, which was traced through the solar wind by the low-frequency type II radio burst detected by *Wind*/WAVES and was also registered in situ near Earth, was fitted with the decelerating shock model of Reiner et al. (2007) (lower pair curves in Figure 4). Even though our fit formally starts at $1 R_{\odot}$, it does not attempt to describe the CME launch. However, we have considered different assumptions about the initial acceleration of this CME to its maximum speed of about 3400 km s^{-1} and estimated, from similar analyses, that this did not change the projected liftoff time from 15:20.9 UT by more than about 1 minute. Although this analysis provides a liftoff time of the CME of 15:20.9 UT, the driven shock would not be expected to form in the corona until somewhat later. In fact, the metric type II burst at 15:24–15:27 UT (Figure 3) is the first evidence for the formation of a shock in the corona.

There is a longstanding controversy concerning the origin of coronal shocks, whether they are all produced by CMEs or whether at least some of them are blast wave shocks that originate with flares (e.g., Vrřnak & Cliver 2008, and references therein). In our analysis above, we assumed that the CME-driven shock that generated the decametric–kilometric type II also generated the first metric type II emissions shown in Figure 3. This assumption provided a constraint on the projected liftoff time of the CME and required that the metric type II emissions must have been generated by the CME-driven shock as it passed through an enhanced density region, such as a coronal streamer, as indicated by the upper dashed curves in Figure 4. While an enhancement factor of 24 may seem excessive for a coronal streamer, Reiner et al. (2003) point out that there are difficulties in estimating the densities of confined structures, like coronal streamers, from white light observations because it is not known how the density is distributed along the line of sight. Polarization brightness inversion techniques generally underestimate the densities in streamers.

On the other hand, it is possible that the first metric type II burst may have been generated by a distinct, flare-induced blast wave, instead of the CME-driven shock. In that case, the kinematic parameters of that shock cannot be uniquely determined,

since the origin time of that shock is unknown. The observed frequency drift rate can be fitted with a number of different shock kinematic and coronal density model parameters. For example, the observed frequency drift can be fitted with a shock, originating at 15:22.7 UT and propagating with a speed of 1350 km s^{-1} through a $0.9 \times$ Saito model corona, i.e., for this scenario it would not be necessary for the blast wave shock to propagate through an enhanced density region of the corona. Such ambiguity might be eliminated if we had the visibility data in the metric radio band, at least like the old data of the Culgoora radioheliograph at $\sim 40 \text{ MHz}$ (e.g., Gergely et al. 1984, their Figure 5 illustrating the locations of different radio emissions produced by a solar eruption in the vicinity of a coronal streamer).

The model frequency–time profile of Figure 4 (upper pair of curves) indicates that three high-frequency type II emission episodes may be caused by a common driver. However, we do not know how a single shock interacting with a continual structure like a coronal streamer could produce such intermittent type II emission. It is not clear that the second metric type II burst, the one associated with the presence of the “herringbone” structure shown in Figure 3, could have been produced by the same CME-driven shock as the other type IIs. Furthermore, a metric type II may be produced not only by a CME bow shock or by a flare blast wave, but also by expanding loops of different scales, as observed in other events by Klein et al. (1999) and Klassen et al. (1999), as well as by CME–streamer interaction (Cho et al. 2008, their Figure 11). The “herringbone” emissions may require a distinct driver propagating transverse to the open magnetic field lines, as could happen when the CME encounters a coronal streamer. The number and nature of type IIs in the corona may be relevant for the subsequent acceleration of SEPs during the main phase of the event.

The close association between major SEP events with western hemisphere metric type IIs accompanied by decametric–hectometric type II emission (Cliver et al. 2004; Gopalswamy et al. 2005) and a lack of SEPs from radio-silent solar eruptions (Marqué et al. 2006) supports the general idea that both the flare/CME liftoff processes in solar corona and the interplanetary shock are essential ingredients of the SEP production in a gradual event. The observations reported in this paper indicate that while the first, helium-rich phase of the major SEP event is dominated by SEPs originating from the eruption core, the event’s main phase is associated with interplanetary shock that accelerates ions from a distinct, helium-poor seed particle population: $\text{He}/p \sim 0.01$. A very low helium abundance in coronal streamers, the CME–streamer interaction indicated by the streamer displacement seen in the *SOHO*/LASCO images of the 2000 April 4 eruption, the open magnetic field topology of coronal streamers, and the inferred accessibility of the interplanetary space for coronal particles during the first ≈ 40 min of the 2000 April 4 event all make the CME–streamer interaction a plausible candidate source of the low-energy seed particles for the main-phase SEP acceleration at the CME–shock complex in the solar wind.

We have analyzed the first phase of the SEP production in the 2000 April 4 event and find a remarkable time coincidence between (1) the timing of the type III bursts, (2) the release profiles of relativistic electrons, and (3) the release profile of helium-rich SEPs. A straightforward interpretation is that the SEP event started with particle emission originating from the CME’s helium-rich core and that those coronal particles escaped into the interplanetary medium before the start of the second, interplanetary phase of this major SEP event. The

interplanetary shock acceleration through the deka–MeV range proceeded for ~ 5 hr after the event’s first phase considered here, until the interplanetary CME finally slowed down to below $\sim 1000 \text{ km s}^{-1}$ (Kocharov et al. 2009).

A two-phase production of SEPs could also be observed when the spacecraft is magnetically connected to a solar area apart from the eruption’s core. However, the first-phase production properties in such an event are expected to be distinct. Torsti et al. (1999) reported on a gradual SEP event associated with an eastern CME, when *SOHO* was magnetically connected to the western periphery of the solar eruption. In that event, the first-phase SEPs had a hard spectrum but were not rich in helium ($\text{He}/p \sim 0.005$), and the first particles’ release was delayed for the EIT-wave transit time from the eruption’s center to the root of the interplanetary magnetic field line connected to *SOHO*. Hence, the coronal phase acceleration may proceed not only in the CME’s helium-rich core but also in distant parts of the solar corona and release of those particles could be due to the continual magnetic reconnection and magnetic field line “opening” associated with the EIT wave. The coronal phase of SEP production seems to be a global phenomenon, whose appearance depends however on the heliocentric angular distance between the eruption’s center and the SEP vantage point.

We acknowledge the extensive efforts of our referee to improve this manuscript. We thank Henry Aurass and Marian Karlicky for supplying the meterwave and microwave data from the Tremisdorf radio observatory of AIP and the Onrejov Observatory, and Jim Ryan is appreciated for commenting on the CGRO data. *SOHO* is a project of international cooperation between ESA and NASA.

REFERENCES

- Bastian, T. S., Benz, A. O., & Gary, D. E. 1998, *ARA&A*, **36**, 131
- Bieber, J. W., Matthaeus, W. H., Smith, C. W., Wanner, W., Kallenrode, M.-B., & Wibberenz, G. 1994, *ApJ*, **420**, 294
- Bochsler, P. 1998, *Space Sci. Rev.*, **85**, 291
- Bougeret, J. L., et al. 1995, *Space Sci. Rev.*, **71**, 231
- Cane, H. V., Erickson, W. C., & Prestage, N. P. 2002, *J. Geophys. Res.*, **107**, 1315
- Cane, H. V., Mewaldt, R. A., Cohen, C. M. S., & von Rosenvinge, T. T. 2006, *J. Geophys. Res.*, **111**, A06S90
- Cane, H. V., von Rosenvinge, T. T., Cohen, C. M. S., & Mewaldt, R. A. 2003, *Geophys. Res. Lett.*, **30**, 12
- Cho, K.-S., Bong, S.-C., Kim, Y.-H., Moon, Y.-J., Dryer, M., Shanmugaraju, A., Lee, J., & Park, Y. D. 2008, *A&A*, **491**, 873
- Cliver, E. W. 1996, in AIP Conf. Proc. 374, High Energy Solar Physics, ed. R. Ramaty, N. Mandzhavidze, & X.-M. Hua (New York: AIP), 45
- Cliver, E. W., Kahler, S. W., & Reames, D. V. 2004, *ApJ*, **605**, 902
- Cohen, C. M. S., et al. 2005, *J. Geophys. Res.*, **110**, A09S16
- Cohen, O., Attrill, G. D. R., Manchester, W. B., & Wills-Davey, M. J. 2009, *ApJ*, **705**, 587
- Delaboudinière, J.-P., et al. 1995, *Sol. Phys.*, **162**, 291
- Feldman, U. 1998, *Space Sci. Rev.*, **85**, 227
- Geiss, J. 1998, *Space Sci. Rev.*, **85**, 241
- Gergely, T. E., et al. 1984, *Sol. Phys.*, **90**, 161
- Gloeckler, G., & Geiss, J. 1989, in AIP Conf. Proc. 183, Cosmic Abundances of Matter, ed. C. J. Waddington (New York: AIP), 49
- Gopalswamy, N. 2003, *Geophys. Res. Lett.*, **30**, 8013
- Gopalswamy, N., Aguilar-Rodríguez, E., Yashiro, S., Nunes, S., Kaiser, M. L., & Howard, R. A. 2005, *J. Geophys. Res. (Space Phys.)*, **110**, A12S07
- Hansteen, V. H., Leer, E., & Holzer, T. E. 1997, *ApJ*, **482**, 498
- Klassen, A., Aurass, H., Klein, K.-L., Hofmann, A., & Mann, G. 1999, *A&A*, **343**, 287
- Klecker, B., et al. 2006, *Space Sci. Rev.*, **123**, 217
- Klein, K.-L., Khan, J. I., Vilmer, N., Delouis, J.-M., & Aurass, H. 1999, *A&A*, **346**, L53

- Kocharov, L., Kovaltsov, G. A., Torsti, J., & Huttunen-Heikinmaa, K. 2005, *J. Geophys. Res.*, **110**, A12S03
- Kocharov, L., Laitinen, T., Al-Sawad, A., Saloniemä, O., Valtonen, E., & Reiner, M. J. 2009, *ApJ*, **700**, L51
- Kozlovsky, B., & Ramaty, R. 1974, *ApJ*, **191**, L43
- Laming, J. M., & Feldman, U. 1994, *ApJ*, **426**, 414
- Laming, J. M., & Feldman, U. 2001, *ApJ*, **546**, 552
- Lynch, B. J., Zurbuchen, T. H., Fisk, L. A., & Antiochos, S. K. 2003, *J. Geophys. Res.*, **108**, 1239
- Mandzhavidze, N., Ramaty, R., & Kozlovsky, B. 1997, *ApJ*, **489**, L99
- Mandzhavidze, N., Ramaty, R., & Kozlovsky, B. 1999, *ApJ*, **518**, 918
- Mann, G., Aurass, H., Voigt, W., & Paschke, J. 1992, in Proc. 1st SOHO Workshop: Coronal Streamers, Coronal Loops, and Coronal and Solar Wind Composition, ed. C. Mattok (Paris: ESA), *ESAP-348*, 129
- Mann, G., & Klassen, A. 2005, *A&A*, **441**, 319
- Marqu e, C., Posner, A., & Klein, K.-L. 2006, *ApJ*, **642**, 1222
- Mason, G. M., Desai, M. I., Cohen, C. M. S., Mewaldt, R. A., Stone, E. C., & Dwyer, J. R. 2006, *ApJ*, **647**, L65
- Murphy, R. J., Share, G. H., Grove, J. E., Johnson, W. N., Kinzer, R. L., Kurfess, J. D., Strickman, M. S., & Jung, G. V. 1997, *ApJ*, **490**, 883
- M uller-Mellin, R., et al. 1995, *Sol. Phys.*, **162**, 483
- Neugebauer, M. 1981, *Fundam. Cosm. Phys.*, **7**, 131
- Neugebauer, M., & Goldstein, R. 1997, in *Coronal Mass Ejections*, ed. N. Crooker, J. A. Joselyn, & J. Feynman (Geophys. Monograph 99; Washington, DC: AGU), 245
- Ng, C. K., Reames, D. V., & Tylka, A. J. 1999, *Geophys. Res. Lett.*, **26**, 2145
- Ramaty, R., et al. 1978, in Proc. 2nd Skylab Workshop on Solar Flares (Boulder Colorado: NASA), chap. 4
- Raymond, J. C., et al. 1997, *Sol. Phys.*, **175**, 645
- Reames, D. V. 1999, *Space Sci. Rev.*, **90**, 413
- Reames, D. V., Ng, C. K., & Tylka, A. J. 2000, *ApJ*, **531**, L83
- Reiner, M. J., Kaiser, M. L., & Bougeret, J.-L. 2007, *ApJ*, **663**, 1369
- Reiner, M. J., Vourlidas, A., Cyr, O. C. St., Burkepile, J. T., Howard, R. A., Kaiser, M. L., Prestage, N. P., & Bougeret, J.-L. 2003, *ApJ*, **590**, 533
- Saito, K. 1970, *Ann. Tokyo Astron. Obs.*, **12**, 53
- Share, G. H., & Murphy, R. J. 1997, *ApJ*, **485**, 409
- Share, G. H., & Murphy, R. J. 1998, *ApJ*, **508**, 876
- Torsti, J., et al. 1995, *Sol. Phys.*, **162**, 505
- Torsti, J., Kocharov, L. G., Teittinen, M., & Thompson, B. J. 1999, *ApJ*, **510**, 460
- Van Hollebeke, M. A. I. 1975, Proc. 14th International Cosmic Ray Conf. (M unchen: Max-Planck-Institut f ur Extraterrestrische Physik), 5, 1563
- Vr snak, B., & Cliver, E. W. 2008, *Sol. Phys.*, **253**, 215